Word Count: 4,665

Revision 2

Cryogenic Heat Capacity Measurements and Thermodynamic Analysis of Lithium Aluminum Layered Double Hydroxides (LDHs) with Intercalated Chloride

K. Jayanthi,[1] Grace Neilsen,[2] Peter F. Rosen,[2] Clark I. Andersen, [2] Matthew S. Dickson, [2] Samuel F. Evans,[3,4] M. Parans Paranthaman,[3,4] Brian F. Woodfield,[2] Alexandra Navrotsky[1]*

[1] School of Molecular Sciences and Center for Materials of the Universe, Arizona State University, Tempe, AZ 85287, United States
[2] Department of Chemistry and Biochemistry, Brigham Young University, Provo, UT 84602, United States
[3] Chemical Sciences Division, Oak Ridge National Laboratory, Oak Ridge, TN 37831, United States
[4] The Bredesen Center for Interdisciplinary Research and Graduate Education, The University of Tennessee, Knoxville, TN 37996, United States

Abstract: Lithium aluminum chloride layered double hydroxide ([Li-Al-Cl] LDH) sorbents selectively recover lithium from geothermal brines, paving the way for increased domestic production of lithium for rechargeable batteries. In this work, cryogenic heat capacity measurements (C_p) were performed from 1.8 to 300 K on several undoped and Fe-doped [Li-Al-Cl] LDH samples with a generalized compositions $Li_{1-x}Al_2(OH)_6Cl_{1-x}$ (undoped) and $Li_xFe_yAl_{2-y}(OH)_6Cl_x$ (Fe-doped). Thermodynamic functions were generated from these measurements, and values of $S°_{298.15}$ are reported based on both the C_p measurements and configurational entropy ($S°_{config}$) arising from positional disorder in the layered structure. These results are combined with previous enthalpy of formation ($\Delta H°_f$) measurements to calculate the Gibbs energy of formation ($\Delta G°_f$) for the samples. In these samples, a higher water content results in a less negative $\Delta G°_f$ when doped and undoped samples are considered separately. Limited iron substitution for aluminum results in the most negative $\Delta G°_f$, but a larger dopant amount destabilizes the LDH structure. One of the samples had an anomaly in the heat capacity from 210 to 300 K, which is likely related to movement of water in the structure due to the large H_2O/Cl^- ratio and the presence of vacancies in the interlayer where H_2O resides. This indicates that the interactions between these species in the interlayer play an important role in stabilizing the LDH structure, and this effect should be further studied using different water/anion ratios.

Keywords: layered double hydroxides; heat capacity; entropy; Gibbs energy; lithium extraction

Introduction

As lithium-ion batteries become increasingly prevalent in technology, novel methods of lithium extraction are needed to meet the increasing demand for lithium (Grosjean et al., 2012). Lithium has typically been obtained through mining lithium ores, and there are continuing efforts to develop simple and inexpensive methods for the recovery of lithium from natural sources. Researchers are beginning to explore the possible extraction of lithium from aqueous sources such as geothermal brines because these natural sources contain an almost unlimited supply of lithium, albeit in low concentrations (Li et al., 2018). A variety of sorbent materials with ion exchange properties are currently under investigation for use in lithium extraction (Ventura et al., 2018). Any viable sorbent must show a high selectivity for Li^+ over Na^+ and K^+, as both are more abundant than Li^+ in these brines (Paranthaman et al., 2017). Layered double hydroxides containing lithium and chloride, denoted as [Li-Al-Cl] LDHs, are potential materials for Li^+ ion capture because of their strong preference for lithium over larger alkali ions, low cost, environmental friendliness, potential scalability, and easy regeneration (Paranthaman et al., 2017).

LDHs are anionic clays with a structure derived from aluminum hydroxide $Al(OH)_3$. The $Al(OH)_3$ structure comprises closely packed hydroxyl ions in which 2/3 of the octahedral sites in alternating layers are occupied by Al^{3+} ions, resulting in a stacking of charge neutral layers having the composition $[Al_{2/3}\square_{1/3}(OH)_2]$ ($\square$=cation vacancy). In [Li-Al-Cl] LDHs, Li^+ fills these vacancies and gives rise to positively charged layers having the composition $[Al_{2/3}Li_{1/3}(OH)_2]^{1/3+}$ (Poeppelmeier and Hwu, 1987). To restore charge neutrality, anions are incorporated in between these metal-hydroxide layers into an interlayer along with water. This yields a class of $Al(OH)_3$-based LDHs with general formula $[Li_xAl_2(OH)_6][A^{n-}]_{x/n}\cdot mH_2O$ ($x \leq 1$), where the A^{n-} may be

OH^-, Cl^-, Br^-, CO_3^{2-}, NO_3^-, SO_4^{2-}, and so on (Paranthaman et al., 2019; Serna et al., 1982). Unlike in II-III LDHs, where cation ordering was corroborated only recently by experimental evidence and structure refinements (Jayanthi and Kamath, 2013; Jayanthi et al., 2015; Jayanthi and Kamath, 2016; Radha et al., 2014), there is abundant evidence from laboratory and synchrotron powder X-ray diffraction (Thiel et al., 1993), neutron powder diffraction (Besserguenev et al., 1997), and ^{14}Al MAS NMR spectra (Hou and Kirkpatrick, 2001) indicating that $[LiAl_2(OH)_6]^+$ units have an ordered array of cations in the metal-hydroxide layer. [Li-Al-Cl] LDHs have, therefore, a generalized formula of $Li_xAl_2(OH)_6Cl_x$ where $0 < x < 1$. [Li-Al-Cl] LDHs can also be doped with Fe^{3+} if they are synthesized in the presence of goethite. The generalized formula of these doped LDHs is $Li_xFe_yAl_{2-y}(OH)_6Cl_x$.

[Li-Al-Cl] LDH is the only material in the LDH family in which delithiation was found to occur (Hou and Kirkpatrick, 2001; Paranthaman et al., 2017; Zhang et al., 2019). Ab initio molecular dynamics (AIMD) simulations showed that this process occurs due to the dynamics of Li^+ motion above ~450 K, while the $[Al_2(OH)_6]$ host layers remain stable up to 1100 K. The calculated large value of the Li^+ diffusion coefficient D, $\sim 3.13 \times 10^{-5}$ cm^2/s, at 500 K and the high stability of the $[Al_2(OH)_6]$ framework suggest a potential application of the partially delithiated $[Li_xAl_2(OH)_6Cl_x]$ $(0 < x < 1)$ as a sorbent of lithium from geothermal brine (Zhang et al., 2019), suggesting a new lithium extraction route. Recently, [Li-Al-Cl] LDH was found to recover 91% of Li^+ from geothermal brine in a single step, with high selectivity over Na^+ and K^+ (Paranthaman et al., 2019; Paranthaman et al., 2017).

Keeping in view the compositional flexibility of the $Al(OH)_3$ based LDHs, [Li-Al] LDHs with variable Li/Al ratios can be envisaged. When the Li/Al ratio is > 0.5, a layer of composition $[Li_{1+x}Al_{2-x}(OH)_6]^{(1-2x)+}$ can be formulated, where the layer charge is lower than that found in the

compound of stoichiometric composition. When the Li/Al ratio is < 0.5, two possibilities arise: either the layers acquire the composition $[Li_{1-x}\square_xAl_2(OH)_6]^{(1-x)+}$ or the layers acquire the composition $[Li_{1-x}Al_{2+x}(OH)_6]^{(1+2x)+}$. In the former case, the layer charge is lower than in the compound of stoichiometric composition, while in the latter case it is higher (Rajamathi et al., 2001). Given the structural complexity and compositional flexibility of [Li-Al-Cl] LDHs, understanding the fundamental chemistry and thermodynamics of these materials is essential to characterizing and improving their ion exchange capabilities.

Despite extensive research centered on LDH synthesis, application, and polytypism, little is known about their thermodynamic stability, which, in the long run, controls cycling life and lithium recovery efficiency (Li et al., 2018; Wu et al., 2019a; Wu et al., 2019b). In our previous works (Wu et al., 2019a; Wu et al., 2019b), we estimated the formation enthalpies of Fe-doped and undoped [Li-Al-Cl] LDHs by considering them as binary mixtures of lithium chloride, gibbsite, and water for undoped LDHs and with goethite, for Fe-doped LDHs. These studies demonstrated the role of the dopant Fe^{3+} and ordered water in increasing the thermodynamic stability of the LDH (Wu et al., 2019a; Wu et al., 2019b). In this work, we present a complete thermodynamic study of selected [Li-Al-Cl] LDHs. Low-temperature heat capacity (C_p) measurements were used to obtain standard entropies ($S°_{298.15}$) of Fe-doped and undoped [Li-Al-Cl] LDHs. These $S°_{298.15}$ were used to calculate entropies of formation ($\Delta S°_f$) which, in combination with enthalpy of formation data ($\Delta H°_f$) obtained from our previous reports (Wu et al., 2019a; Wu et al., 2019b), yield the Gibbs energies of formation ($\Delta G°_f$) presented in this work. These $S°_{298.15}$ and $\Delta G°_f$ provide insights into the stability of [Li-Al-Cl] LDHs as a function of their water content and dopant concentration.

Experimental Methods

Synthesis and characterization (including powder x-ray diffraction, inductively coupled plasma-optical emission spectroscopy, differential scanning calorimetry, and thermogravimetry measurements) of these LDHs were performed previously (Wu et al., 2019a; Wu et al., 2019b). Because the degree of hydration in LDHs depends on the age of the sample and the humidity of the atmosphere in which they were stored, water content was remeasured using a Mettler Toledo TGA/DSC 1 STARe System prior to further measurement. Approximately 5–30 mg of sample were heated from 303 to 1273 K at 10 K/min in helium atmosphere. The temperature of 973 K was chosen as the cutoff for calculating water content because, at this temperature, all of the TGA curves were at a plateau before lithium loss occurs above 1023K (Wu et al., 2019b). The uncertainty of the balance is 0.1 μg. TGA curves are given in Figure S1, and percentage mass loss (at 973 K) and water contents based on these curves are given in Table 1.

The Li and Cl content in LDH 1 is unexpectedly high and gives a Li/Al ratio of 0.68 without a reduction in the amount of Al. This suggests there may be a secondary phase of LiCl present. Therefore, we remeasured this sample using powder X-ray diffraction (PXRD) to check for the presence of an LiCl secondary phase (PXRD measurements have previously been performed on all samples (Wu et al., 2019a; Wu et al., 2019b)). The results from this measurement, given in Figure S2, show evidence of a LiCl secondary phase, and thus we report the composition of LDH 1 to be $LiAl_2(OH)_6Cl{\cdot}3.20H_2O{\cdot}0.36LiCl$ instead of the previously reported formula of $Li_{1.36}Al_2(OH)_6Cl_{1.36}{\cdot}3.26H_2O$. (Note that the water content was requantified prior to heat capacity measurements.)

Heat capacity measurements were performed with a Quantum Design Physical Property Measurement System (PPMS) in zero magnetic field from 1.8 to 300 K. Each sample was prepared according to a method devised for measuring the heat capacities of insulating powders

(Shi et al., 2011; Shi et al., 2010). Approximately 12 mg of each sample was enclosed in a copper cup (0.025 mm thick, 99.999% purity from Alfa Aesar). A small copper coil was also inserted into each cup to ensure uniform heating throughout the sample (Rosen and Woodfield, 2020). After being pressed into a pellet, each sample was attached to the sample holder using a small amount of Apiezon N grease and placed in the PPMS. An addenda measurement was performed before each measurement to account for the C_p of the sample holder and the grease. This method has an estimated accuracy of ± 2% below 10 K and ± 1% from 10 to 300 K. Samples were measured under vacuum, and we assume water loss was negligible. For LDH 1, calculated heat capacity of the LiCl secondary phase based on measurements done by Shirley (1960) was subtracted off to yield C_p for just the LDH. This secondary LiCl phase is most likely present as a hydrate on these samples, which would increase the heat capacity we need to subtract off, but we cannot differentiate between water associated with the LiCl secondary phase and with the LDH. We assume, therefore, that the secondary phase in this sample behaves as anhydrous LiCl. This assumption does increase the error of LDH 1 although it is difficult to quantify this increase.

Results

As seen in the TGA curves, water comes off the LDHs in several steps. Physically absorbed water first comes off below 423 K. Chemically bound water intercalated in the interlayer then comes off next between 423–523 K (Wu et al., 2019b). The mass loss at 523–623 K corresponds to dehydroxylation (Besserguenev et al., 1997). The mass loss above 1023 K is associated with further sample decomposition. Wu et al. (2019) reported this same general pattern of steps for water loss in [Li-Al-Cl] LDHs, and they correlated the high temperature mass loss with the loss of lithium as Li_2O (Wu et al., 2019b).

The measured C_p data are given per mole in Tables S1-S5 and presented in Figure 1 (LDH 1, 2, 4, and 5) and Figure 2 (LDH 3). LDH 3 is featured separately for clarity. There are several notable features in these measurements. First, there is a broad anomaly in the heat capacity of LDH 3 from approximately 210 to 300 K. Second, the low temperature heat capacities of LDH 4 and LDH 5, which both contain Fe^{3+}, flatten out rather than approach zero below 3 K. This is apparently due to the Fe^{3+} dopant giving rise to a Schottky anomaly, further discussed below. Finally, the heat capacities of the three undoped LDHs have approximately the same magnitude, while the Fe^{3+}-doped LDHs have significantly lower heat capacities.

Discussion

Heat capacity curve fitting

To gain further information from the heat capacity measurements, the measured C_p were fit using theoretical functions in two distinct temperature regions (T < 11 K and T > 40 K), and an orthogonal polynomial was used as a smooth transition between the two regions. These fits are shown with the experimental data in Figure 1 and Figure 2.

Below 10 K, the C_p of the undoped LDHs (LDH 1, LDH 2, and LDH 3) are represented by:

$$C_{p,m} = \gamma T + B_3 T^3 + B_5 T^5 + B_7 T^7 \quad (1)$$

where γ, B_3, B_5, and B_7 are constants obtained from fitting the data, and these parameters are given in Tables S6. The B_3T^3, B_5T^5, and B_7T^7 terms represent the lattice contribution to the C_p (Gopal, 1966; Majzlan et al., 2003; Shi et al., 2011). A linear term, γT, is usually seen in conductors to represent electronic heat capacity; however, these materials are insulators. In insulators, a linear term can account for lattice vacancies or for lattice impurities (Neilsen et al.,

178 2020; Schliesser et al., 2015). In these LDHs samples, there can be vacancies in both the metal-
179 hydroxide layers and interlayers, so it seems likely that these give rise to the linear term.

180 Substitution of Fe^{3+} into the metal-hydroxide layer of the doped LDHs, LDH 4 and
181 LDH 5, results in Schottky anomalies in the low temperature heat capacity of these two samples.
182 These Schottky anomalies arise due to the splitting of the paramagnetic moment of the Fe^{3+}
183 nuclei into a non-degenerate system of energy levels (Shi et al., 2011; Cooke et al., 1956), and
184 we expect to see this anomaly as a small peak in the heat capacity below 10 K. Due to the
185 temperature range of our measurements, we see this as a slight upturn below 2 K (see Figure 3).
186 This upturn is similar to the Schottky anomaly in the heat capacity of $FeOOH{\cdot}0.027H_2O$ (Snow
187 et al., 2013), the same compound used as the source of the Fe^{3+} dopant in these samples. To
188 account for this, LDH 4 and LDH 5 were fit using Eq. 1 with an added Schottky term taking the
189 form:

190 $$C_{sch} = n_{sch} R \left(\frac{\theta}{T}\right)^2 g \frac{\exp(\theta/T)}{[1+g\exp(\theta/T)]^2} \quad (2)$$

191 where n_{sch} represents the number of nuclei contributing to the anomaly, g represents the
192 degeneracy of the system, and θ is the energy gap between the energy levels in K. The
193 parameters used to fit LDH 4 and LDH 5 below 10 K are given in Table S7. Because a rigorous
194 analysis of this anomaly is beyond the scope of this paper, the simplest possible model (a two-
195 level system) was used. The resulting fit matches the data well and is sufficient for the purpose
196 of calculating thermodynamic functions from the C_p data.

197 The medium temperature regions were fit to 8th order orthogonal polynomials, which do
198 not have a theoretical basis but are used to provide a smooth overlap between the low and high
199 temperature functions (Justice, 1969):

200 $$C_{p,m} = \sum_{i=0}^{8} a_i T^i \quad (3)$$

The polynomial coefficient values, a_i, are also given in Tables S6-7.

Heat capacities in the high temperature region were fit to a combination of Debye and Einstein functions, which represent the contribution of lattice vibrations at higher temperatures:

$$C_{p,m} = m \cdot D(\Theta_D/T) + n_1 \cdot E(\Theta_{E1}/T) + AT \quad (4)$$

where $D(\Theta_D/T)$ is a Debye function, $E(\Theta_{E1}/T)$ is an Einstein function, and m and n_1 represent the number of Debye or Einstein oscillators with characteristic temperatures of Θ_D and Θ_{E1} respectively (Gopal, 1966). The linear term, A, included in this equation acts as a correction between the C_v modeled by the Debye and Einstein functions and the C_p measured here. This equation was used to fit all the LDH samples except LDH 3.

LDH 3 exhibits a transition in the heat capacity between 210 and 300 K separate from the lattice heat capacity; therefore, it required a different fitting approach. Because Debye and Einstein functions only model lattice heat capacity, a fit of the LDH 3 lattice was generated using data from 53.08 K to 201.65 K using a sum of one Debye function and one Einstein function. This fit was extrapolated up to 300 K to represent the smoothed lattice heat capacity (included in Figure 2), and values for Θ_D, Θ_E, m, and n for this fit are included in Table S6.

To calculate the thermodynamic values of the transition in LDH 3, values from the C_p fit of the lattice from 210 K to 300 K were subtracted from a cubic spline fit of the measured C_p. The calculated enthalpy of the transition from our data up to 300 K is 1.072 ± 0.02 kJ·mol^{-1}, and the entropy is 4.20 ± 0.08 J·mol^{-1}·K^{-1}. Because the transition does not seem to be complete at 300 K, a linear segment with the same slope as the spline at 300 K was used to approximate the high T region of the transition (up to 310 K), and this was used to calculate the total enthalpy and entropy of the transition. The calculated enthalpy of the transition using this additional

223 extrapolation is 1.13 ± 0.02 kJ·mol^{-1}, and the entropy is 4.40 ± 0.09 J·mol^{-1}·K^{-1}.
224 Thermodynamic functions from the spline fit are included from 210 K to 300 K in Table S10.

225 Because LDH 3 had a composition similar to those of the other samples, the presence of a
226 transition is somewhat surprising. Transitions in this region in C_p measurements often result from
227 the movement of water inside a structure (Hemingway and Robie, 1984), so it seems likely that
228 the transition in LDH 3 is also related to water movement. Previous studies have shown that
229 water molecules in the interlayer are in an intermediate state between liquid and solid (Allada et
230 al., 2005), and studies on similar LDH samples showed that the water is not localized in an ice-
231 like state but possesses some rotational freedom in the interlayer, which means some water
232 molecules are strongly bound and some are loosely held in the LDH (Radha et al., 2014). LDH 3
233 does not have the highest water content, but it does have a higher water to anion ratio in the
234 interlayer than any of the other samples. (Note that while LDH 1 nominally has the largest
235 water/anion ratio in the interlayer, this ratio is likely smaller due to possible hydration of the
236 LiCl secondary phase.) Structural studies have shown that as water is added to the interlayer of
237 [Li-Al-Cl] LDHs, it first forms hydration spheres around the anions and then hydrogen bonds
238 with the hydroxyl groups on different metal-hydroxide layers (Radha et al., 2014). In this case, a
239 higher water/anion ratio could result in more loosely bound water, not incorporated in hydration
240 spheres, that can move between interstitial sites. This movement at temperatures above 200 K
241 could give rise to a transition when the water/anion ratio is sufficiently high, as in LDH 3. Note
242 that the presence of vacancies in the interlayer may also play an important role in this transition.
243 As discussed below, LDH 3 has vacancies in the interlayer, while LDH 1 and LDH 2 do not.
244 However, LDH 4 and LDH 5 also have vacancies but exhibit no transition in their high
245 temperature heat capacities. This suggests that although the presence of vacancies may be

246 required for this transition to occur, the presence of vacancies by itself is not enough to cause a
247 transition.

248 **Standard Entropy Calculations**

249 In the absence of electronic and magnetic effects, the standard entropy of a solid ($S°_{298.15}$)
250 is given as the sum of the vibrational and configurational contributions, $S°_{298.15} = S°_{vib} + S°_{config}$.
251 In this equation, the vibrational (lattice) entropy of the LDHs is calculated from the C_p as
252 follows:

253 $$S°_{vib} = \int_0^T \frac{C_p}{T} dT \quad (5)$$

254 where C_p is the heat capacity. The vibrational entropies ($S°_{vib}$) at 298.15 K calculated from the
255 measured C_p are also reported in Table 2 for all the [Li-Al-Cl] LDHs

256 In addition to vibrational entropy, $S°_{vib}$, which is calculated from the C_p measurement and
257 given in Table 2, these LDHs also have configurational entropy, $S°_{config}$, which arises due to
258 disordered arrangements of cations, vacancies, anions, and water that further stabilize the LDH
259 structure. $S°_{config}$ can be calculated using a model of two sub-lattices: the metal-hydroxide layer
260 and the interlayer. The calculation provided here is modified from the $S°_{config}$ calculation used by
261 Poonoosamy et al. (2018). The metal-hydroxide layer consists of the $Al(OH)_3$ structure with Li^+
262 occupying some vacant sites and Fe^{3+} substituting into some Al^{3+} sites in the doped LDHs. The
263 interlayer contains a random arrangement of Cl^-, H_2O, and vacancies. For Li/Al ratio < 0.5, the
264 vacancy concentration in the metal-hydroxide layer (V_{MHL}) can be calculated using equations (6)
265 and (7) for doped and undoped LDHs.

266 $$V_{MHL} = 3 - x - y \quad (6)$$

This is the peer-reviewed, final accepted version for American Mineralogist, published by the Mineralogical Society of America.
The published version is subject to change. Cite as Authors (Year) Title. American Mineralogist, in press.
DOI: https://doi.org/10.2138/am-2021-7935. http://www.minsocam.org/

$$V_{MHL} = 3 - x - y - z \quad (7)$$

where x, y, and z are moles of Li^+, Al^{3+} and Fe^{3+}. In undoped LDHs, Li^+ occupies the vacant sites and the Al^{3+} sites can be occupied by Al^{3+}. Therefore, the configurational entropy of the metal-hydroxide layer in undoped LDHs with Li/Al ratio < 0.5 is given as:

$$S°_{\text{config, MHL}} = -RN_T[X_{Li}lnX_{Li} + X_{VL}lnX_{VL}] \quad (8)$$

where R is the gas constant 8.314 $J \cdot mol^{-1} \cdot K^{-1}$, N_T is the total moles of the mixing species, and X_{Li} and X_{VL} are the mole fractions of Li^+ and vacancies in these sites.

In doped LDHs, the configurational entropy arising from Li^+ - vacancy disorder is calculated using Eq. 8, but because either Al^{3+} or Fe^{3+} can occupy the Al^{3+} sites, an additional term is added to $S°_{\text{config}}$:

$$S°_{\text{config, MHL}} = -RN_T[X_{Al}lnX_{Al} + X_{Fe}lnX_{Fe}] \quad (9)$$

where X_{Al} and X_{Fe} are the mole fractions of Al^{3+} and Fe^{3+} in these sites. Eq. 8 and 9 contribute to $S°_{\text{config,MHL}}$ in doped LDHs.

The configurational entropy of the interlayer is based on the number of vacant sites, anion sites, and water sites, assuming they are closely packed. For LDHs with $(Cl^- + H_2O) < 3$, the fraction of vacant sites (V_{IL}) in the interlayer, is calculated as:

$$V_{IL} = 3 - n - m \quad (10)$$

where n and m are the moles of Cl^- and H_2O, respectively. The $S°_{\text{config,IL}}$ is given as:

$$S°_{\text{config,IL}} = -RN_T[X_AlnX_A + X_WlnX_W + X_{VI}lnX_{VI}] \quad (11)$$

where X_A, X_w, and X_{VI} are the mole fractions of Cl^-, H_2O, and vacancies in the interlayer. While the number of vacancies can be determined using Eq. 10, the LDH structure can easily accommodate excess water. Water molecules along with anions play a major role in holding the metal-hydroxide layers intact and thus stabilizing the LDH structure. In the case of $(Cl^- + H_2O) > 3$, we take the vacancy concentration to be zero. Thus, the calculation of $S°_{config,IL}$ does not include the X_{VI} term in Eq. 11 and N_T is the sum of Cl^- and H_2O in the sample.

While these calculations provide a useful approximation for $S°_{config}$, there are some limitations and exceptions. Equations (8), (9), and (11) represent a maximum $S°_{config}$, and any ordering in the metal-hydroxide layer would diminish this contribution (Poonoosamy et al., 2018). Another issue is that LDH 2 has an Li/Al ratio > 0.5, indicating an excess of Li^+ and Cl^- likely present as a LiCl secondary phase. Since the excess Li^+ and Cl^- in LDH 2 is small, it was assumed for simplicity that all the Li^+ and Cl^- is inside the metal-hydroxide layer and interlayer respectively, and the vacancy concentrations for both were taken to be zero. The Li/Al ratio in LDH 1 is 0.5, and we likewise assume that there are no vacancies in this sample. Therefore, in LDH 1 and LDH 2, $S°_{config,MHL}$ is taken to be zero since the vacant sites are completely filled with Li^+ and the Al^{3+} sites are only occupied by Al^{3+}.

The calculated $S°_{config}$ values were added to $S°_{vib}$ values from the heat capacity measurements to give $S°_{298.15}$, given in Table 2. Overall, the calculated $S°_{298.15}$ values increase with increasing water content in the interlayer (Figure 4). The chloride and water molecules are assumed to be randomly located in the interlayer region with large site degeneracy due to positional disorder in the interlayer (Besserguenev et al., 1997). This pattern generally holds when the doped and undoped LDHs are considered separately, and the only exception is LDH 3. LDH 3 has significantly higher $S°_{config}$ than expected since it has lower water content than LDH

2. This is due to the three species (Cl^-, H_2O, and vacancies) included in the $S°_{config}$ calculation for the interlayer in LDH 3 as opposed to the two species (Cl^- and H_2O) included in the calculation for the interlayer in LDH 1 and LDH 2. In addition, LDH 3 has a higher $S°_{vib}$ than LDH 2 due to the presence of the heat capacity anomaly.

Thermodynamic calculations

The heat capacity fits in Tables S6 and S7 were used to calculate $\Delta_{\circ}^{T}S_m$, $\Delta_{\circ}^{T}H_m$, and Φ_m, given in Tables S8 – S12. $\Delta S°_f$ was calculated as the entropy difference between the single cation components listed in Table S15 and the $S°_{298.15}$ of the undoped/doped LDH phases. The $\Delta S°_f$ determined was used to calculate the $\Delta G°_f$ values. $\Delta S°_f$ and $\Delta G°_f$ were calculated for all the [Li-Al-Cl] LDHs from binary oxides, ox-hydroxides, and hydroxides at T = 298.15 K, and these values, along with the respective $\Delta H°_f$ used for the calculations, are summarized in Tables 2 (from oxides) and S13 (from ox-hydroxides and hydroxides).

The reported enthalpies are based on dissolution enthalpies measured in our previous work (ΔH_{dissol}) (Wu et al., 2019a; Wu et al., 2019b). Because the dissolution enthalpy of liquid water in 5 N HCl solution is small, it was neglected in our previous calculations. However, in this paper, we have included the ΔH_{dissol} of water based on TGA measurements reported here in all our calculations (Table 1). The formation enthalpies ($\Delta H°_{f,ox}$, $\Delta H°_{f,ox\text{-}hyd}$, and $\Delta H°_{f,hyd}$) in Tables 2 and S13 were recalculated using the adjusted ΔH_{dissol} values in Table 1 and the thermochemical cycle in Table S14. Note that LDHs have $S°_{config}$ while the binary components do not, and this increased disorder helps to stabilize the LDH structure.

In terms of $\Delta G°_f$, the order of stability is: LDH 5 > LDH 3 > LDH 2 > LDH 4 > LDH 1. This trend inversely follows the water contents of the samples if the Fe-doped and undoped

LDHs are considered separately. However, due to the number of competing factors, such as the dopant concentration, the presence of a LiCl secondary phase, and the anomaly in the LDH 3 heat capacity, it is difficult to say for certain whether this trend can be generalized to other compositions.

The $\Delta G°_f$ calculations reported here support the findings in our previous studies (Wu et al., 2019a; Wu et al., 2019b) that a small amount of iron doping significantly increases LDH stability, with LDH 5 having the most negative $\Delta G°_f$ value (Tables 2 and S13). This also aligns with previous studies on the structural stability of LDHs that have shown Fe^{3+} LDHs to have greater thermodynamic stability than Al^{3+} (Boclair and Braterman, 1999). Despite the increase in $S°_{298.15}$ with higher dopant content, a higher level of Fe^{3+} doping appears to be less stabilizing, with LDH 4 having one of the least negative $\Delta G°_f$. This also agrees with our prior work (Wu et al., 2019a; Wu et al., 2019b), and because the stability trend is opposite to the $S°_{298.15}$ trend, we can conclude that the destabilization by increased iron doping is enthalpically driven.

Implications

By understanding the thermodynamic trends of these materials, we can isolate which features will most likely impact the stability and longevity of [Li-Al-Cl] LDHs. Our $\Delta G°_f$ results agree with Wu et al. (2019b) that a small amount of dopant stabilizes the LDH, and this could give Fe-doped [Li-Al-Cl] LDHs a longer lifetime for commercial use. Water also seems to influence $\Delta G°_f$, though establishing a trend would require further study, and our heat capacity measurements show how the molar amount of water is not the only factor to consider. The transition-like anomaly in the heat capacity of LDH 3 indicates that the behavior of water is dependent on the both where the water is in the interlayer with respect to the anions and the

353 concentration of anions in the interlayer. Because previous studies have correlated water
354 ordering and water retainment with lithium recovery efficiency, this phenomenon should be
355 further studied. As a next step, one should explore the stability and water behavior of [Li-Al]
356 LDHs with different water/anion ratios. These studies would also clarify the role of anions in
357 stabilizing the LDH structure. Understanding the dynamics of the interlayer and how the water
358 and anions affect the thermodynamics of LDHs is crucial for selecting
359 the most stable LDH composition to be used as a sorbent for Li^+ extraction from geothermal
360 brines and other aqueous sources. Such data will also further elucidate the formation of LDH
361 phases in the geothermal and aqueous geochemical environment.

362 **Acknowledgements**

363 The heat capacity measurements and analyses were supported by the U.S. Department of
364 Energy under grant DE-SC0016446. Synthesis and further thermodynamic analysis research
365 were supported by the Critical Materials Institute, an Energy Innovation Hub funded by the U.S.
366 Department of Energy, Office of Energy Efficiency and Renewable Energy, Advanced
367 Manufacturing Office. S.F.E. is grateful for a fellowship from the Bredesen Center for
368 Interdisciplinary Graduate Education. Funding for RET (Research Experiences for Teachers)
369 participant C. I. A. was provided by the National Science Foundation Chemistry and
370 Biochemistry REU Site to Prepare Students for Graduate School and an Industrial Career under
371 award CHE-1757627.

372 This manuscript has been authored by UT-Battelle, LLC under Contract No. DE-AC05-
373 00OR22725 with the U.S. Department of Energy. The United States Government retains and the
374 publisher, by accepting the article for publication, acknowledges that the United States
375 Government retains a non-exclusive, paid-up, irrevocable, world-wide license to publish or

References

Allada, R.K., Navrotsky, A., and Boerio-Goates, J. (2005) Thermochemistry of hydrotalcite-like phases in the MgO-Al_2O_3-CO_2-H_2O system: A determination of enthalpy, entropy, and free energy. *American Mineralogist*, 90(2-3), 329-335.

Besserguenev, A.V, Fogg, A., Francis, R., Price, S., O'hare, D., Isupov, V., and Tolochko, B. (1997) Synthesis and structure of the gibbsite intercalation compounds $[LiAl_2(OH)_6]$ X {X= Cl, Br, NO_3} and $[LiAl_2(OH)_6]Cl{\cdot}H_2O$ using synchrotron x-ray and neutron powder diffraction. *Chemistry of Materials*, 9(1), 241-247.

Boclair, J.W., and Braterman, P.S. (1999) Layered double hydroxide stability. 1. Relative stabilities of layered double hydroxides and their simple counterparts. *Chemistry of Materials*, 11(2), 298-302.

Cooke, A., Meyer, H., and Wolf, W. (1956) Thermal and magnetic properties of ferric methylammonium sulphate. *Proceedings of the Royal Society of London. Series A. Mathematical and Physical Sciences*, 237(1210), 404-412.

Gopal, E.S.R. (1966) Specific heats at low temperatures. 240 p. Plenum Press, New York.

Grosjean, C., Miranda, P.H., Perrin, M., and Poggi, P. (2012) Assessment of world lithium resources and consequences of their geographic distribution on the expected development

398 of the electric vehicle industry. *Renewable and Sustainable Energy Reviews*, 16(3), 1735-
399 1744.

400 Hemingway, B.S., and Robie, R.A. (1984) Thermodynamic properties of zeolites: low-
401 temperature heat capacities and thermodynamic functions for phillipsite and
402 clinoptilolite. Estimates of the thermochemical properties of zeolitic water at low
403 temperature. *American Mineralogist*, 69(7-8), 692-700.

404 Hou, X., and Kirkpatrick, R.J. (2001) Thermal evolution of the Cl^{-}−$LiAl_2$ layered double
405 hydroxide: A multinuclear MAS NMR and XRD perspective. *Inorganic Chemistry*,
406 40(25), 6397-6404.

407 Jayanthi, K., and Kamath, P.V. (2013) Observation of cation ordering and anion-mediated
408 structure selection among the layered double hydroxides of Cu (II) and Cr (III). *Dalton*
409 *Transactions,* 42(36), 13220-13230.

410 Jayanthi, K., Nagendran, S., and Kamath, P.V. (2015) Layered double hydroxides: proposal of a
411 one-layer cation-ordered structure model of monoclinic symmetry. *Inorganic Chemistry*,
412 54(17), 8388-8395.

413 Jayanthi, K., and Kamath, P.V. (2016) A crystal chemical approach to a cation-ordered structure
414 model for carbonate-intercalated layered double hydroxides. *Crystal Growth & Design*,
415 16(8), 4450-4456.

416 Justice, B.H. (1969) Thermal data fitting with orthogonal functions and combined table
417 generation. The FITAB Program. AEC Cryogenics Project, University of Michigan, Ann
418 Arbor, Michigan.

Li, L., Deshmane, V.G., Paranthaman, M.P., Bhave, R.R., Moyer, B.A., and Harrison, S. (2018) Lithium recovery from aqueous resources and batteries: A brief review. *Johnson Matthey Technology Review*, 62(2).

Majzlan, J., Navrotsky, A., Woodfield, B., Lang, B., Boerio-Goates, J., and Fisher, R. (2003) Phonon, spin-wave, and defect contributions to the low-temperature specific heat of α-FeOOH. *Journal of Low Temperature Physics*, 130(1-2), 69-76.

Neilsen, G., Rosen, P.F., Dickson, M.S., Popovic, M., Schliesser, J., Hansen, L.D., Navrotsky, A., and Woodfield, B.F. (2020) Quantifying oxygen vacancies in neodymium and samarium doped ceria from heat capacity measurements. *Acta Materialia*, 188, 740-744.

Paranthaman, M.P., Bhave, R.R., Moyer, B.A., and Harrison, S. (2019) Composition for recovery of lithium from brines, and process of using said composition. U.S. Patent # 10,266,915, April 23.

Paranthaman, M.P., Li, L., Luo, J., Hoke, T., Ucar, H., Moyer, B.A., and Harrison, S. (2017) Recovery of lithium from geothermal brine with lithium–aluminum layered double hydroxide chloride sorbents. *Environmental Science & Technology*, 51(22), 13481-13486.

Parker, V.B. (1965) Thermal properties of aqueous uni-univalent electrolytes. Dept. of Commerce, National Bureau of Standards, Washington, D.C., U.S.

Poeppelmeier, K.R., and Hwu, S. (1987) Synthesis of lithium dialuminate by salt imbibition. *Inorganic Chemistry*, 26(20), 3297-3302.

Poonoosamy, J., Brandt, F., Stekiel, M., Kegler, P., Klinkenberg, M., Winkler, B., Vinograd, V., Bosbach, D., and Deissmann, G. (2018) Zr-containing layered double hydroxides:

441 Synthesis, characterization, and evaluation of thermodynamic properties. *Applied Clay*
442 *Science*, 151, 54-65.
443 Radha, S., Jayanthi, K., Breu, J., and Kamath, P.V. (2014) Relative humidity-induced reversible
444 hydration of sulfate-intercalated layered double hydroxides. *Clays and Clay Minerals*,
445 62(1), 53-61.
446 Rajamathi, M., Thomas, G.S., and Kamath, P.V. (2001) The many ways of making anionic clays.
447 *Journal of Chemical Sciences*, 113(5-6), 671-680.
448 Rosen, P.F., and Woodfield, B.F. (2020) Standard methods for heat capacity measurements on a
449 quantum design physical property measurement system. *The Journal of Chemical*
450 *Thermodynamics*, 141, 105974.
451 Schliesser, J.M., and Woodfield, B.F. (2015) Lattice vacancies responsible for the linear
452 dependence of the low-temperature heat capacity of insulating materials. *Physical Review*
453 *B*, 91(2), 024109.
454 Serna, C.J., Rendon, J.L., and Iglesias, J.E. (1982) Crystal-chemical study of layered
455 $[Al_2Li(OH)_6]^+ X^- \cdot nH_2O$. *Clays and Clay Minerals*, 30(3), 180-184.
456 Snow, C.L., Lilova, K.I., Radha, A.V., Shi, Q., Smith, S., Navrotsky, A., Boerio-Goates, J., and
457 Woodfield, B.F. (2013) Heat capacity and thermodynamics of a synthetic two-line
458 ferrihydrite, $FeOOH \cdot 0.027H_2O$. *The Journal of Chemical Thermodynamics*, 58, 307-314.
459 Shi, Q., Boerio-Goates, J., and Woodfield, B.F. (2011) An improved technique for accurate heat
460 capacity measurements on powdered samples using a commercial relaxation calorimeter.
461 *The Journal of Chemical Thermodynamics*, 43(8), 1263-1269.

462 Shi, Q., Snow, C.L., Boerio-Goates, J., and Woodfield, B.F. (2010) Accurate heat capacity
463 measurements on powdered samples using a quantum design physical property
464 measurement system. *The Journal of Chemical Thermodynamics*, 42(9), 1107-1115.
465 Shirley, D. (1960) The heat capacity of lithium chloride from 15 to 325 degrees Kelvin. *Journal*
466 *of the American Chemical Society*, 82(15), 3841-3843.
467 Thiel, J., Chiang, C., and Poeppelmeier, K.R. (1993) Structure of lithium aluminum hydroxide
468 dihydrate ($LiAl_2(OH)_7 \cdot 2H_2O$). *Chemistry of Materials*, 5(3), 297-304.
469 Ventura, S., Bhamidi, S., and Hornbostel, M. (2018) Selective recovery of lithium from brines,
470 Proceedings, 43rd workshop on geothermal reservoir engineering. Stanford University.
471 Wu, L., Evans, S.F., Cheng, Y., Navrotsky, A., Moyer, B.A., Harrison, S., and Paranthaman,
472 M.P. (2019a) Neutron spectroscopic and thermochemical characterization of lithium–
473 aluminum-layered double hydroxide chloride: Implications for lithium recovery. The
474 *Journal of Physical Chemistry C*, 123(34), 20723-20729.
475 Wu, L., Li, L., Evans, S.F., Eskander, T.A., Moyer, B.A., Hu, Z., Antonick, P.J., Harrison, S.,
476 Paranthaman, M.P., and Riman, R. (2019b) Lithium aluminum-layered double hydroxide
477 chlorides (LDH): Formation enthalpies and energetics for lithium ion capture. *Journal of*
478 *the American Ceramic Society*, 102(5), 2398-2404.
479 Zhang, Y., Cheng, X., Wu, C., Köhler, J., and Deng, S. (2019) Electronic structure and lithium
480 diffusion in $LiAl_2(OH)_6Cl$ studied by first principle calculations. *Molecules*, 24(14),
481 2667.

482
483

Figure 1. Experimental molar heat capacity and fitted curves from 0 to 300 K for the LDH 1, LDH 2, LDH4, and LDH 5. In this figure, the LiCl secondary phase has been subtracted off the measured heat capacity of LDH 1.

Figure 2. Experimental molar heat capacity and fitted curves from 0 to 300 K for LDH 3. The LDH 3 heat capacity contains a transition above 200 K, and the fit line displayed here for LDH 3 is an extrapolation of the lattice heat capacity calculated using Eq. 4 using the parameters for LDH 3 in Table S6. This fit does not account for the transition.

Figure 3. Experimental molar heat capacity and fitted curves below 10 K for the doped and undoped [Li-Al-Cl] LDHs. LDH 4 and LDH 5 exhibit Schottky anomalies below 2 K.

Figure 4. $S°_{298.15}$ ($J \cdot K^{-1} \cdot mol^{-1}$) vs moles of water in the doped and undoped [Li-Al-Cl] LDHs.

This is the peer-reviewed, final accepted version for American Mineralogist, published by the Mineralogical Society of America.
The published version is subject to change. Cite as Authors (Year) Title. American Mineralogist, in press.
DOI: https://doi.org/10.2138/am-2021-7935. http://www.minsocam.org/

Table 1. Composition and dissolution enthalpy of the LDH samples and the starting materials used to calculate the formation enthalpy calculations.

Sample	Composition	Molecular weights ($g \cdot mol^{-1}$)	TG weight loss%	Li/Al ratio	ΔH_{dissol} ($kJ \cdot mol^{-1}$)
LDH 1[a,b]	$LiAl_2(OH)_6Cl \cdot 3.20H_2O \cdot 0.36LiCl$	271.31	41.14%	0.5	-214.25±1.01[c]
LDH 2[d]	$Li_{1.03}Al_2(OH)_6Cl_{1.03} \cdot 2.47H_2O$	244.17	40.36%	0.51	-183.23±1.42
LDH 3[d]	$Li_{0.73}Al_2(OH)_6Cl_{0.73} \cdot 2.06H_2O$	224.13	40.62%	0.37	-185.72±0.75
LDH 4[d,e]	$Li_{0.57}Fe_{0.44}Al_{1.56}(OH)_6Cl_{0.57} \cdot 1.11H_2O$	212.86	34.85%	0.28	-174.14±0.58
LDH 5[a]	$Li_{0.78}Fe_{0.23}Al_{1.77}(OH)_6Cl_{0.78} \cdot 0.96H_2O$	213.00	33.50%	0.39	-155.66±0.95
Lithium chloride	LiCl				-34.46±1.90
Gibbsite	γ-$Al(OH)_3$				-101.37±0.46
Goethite	α-FeOOH				-43.44±0.95
Water	H_2O				-0.54[f]

[a] Sample reported in Wu et al., 2019b.

[b] Secondary phase (LiCl) is taken into consideration in this paper which was neglected in Wu et al., 2019b.

[c] The LiCl secondary phase has been subtracted off for the ΔH_{dissol} of LDH 1.

[d] Sample reported in Wu et al., 2019a.

[e] Composition was wrongly reported in Wu et al., 2019a and is rectified in this paper; the corresponding $\Delta H°_f$ was calculated.

[f] Calculated from Parker, 1965.

Table 2. Thermodynamic parameters from binary oxides for [Li-Al-Cl] LDHs at T = 298.15 K.

LDH	$\Delta H°_{f,ox}$ ($kJ \cdot mol^{-1}$)	$\Delta S°_{f,ox}$ ($J \cdot K^{-1} \cdot mol^{-1}$)	$\Delta G°_{f,ox}$ ($kJ \cdot mol^{-1}$)	$S°_{vib}$ ($J \cdot K^{-1} \cdot mol^{-1}$)	$S°_{config}$ ($J \cdot K^{-1} \cdot mol^{-1}$)	$S°_{298.15}$ ($J \cdot K^{-1} \cdot mol^{-1}$)
LDH 1	-79.40±2.79	-255.82±5.38	-3.13±2.79	269.20±5.38	19.17	288.37±5.38
LDH 2	-111.06±2.96	-232.35±4.90	-41.78±2.96	245.19±4.90	17.32	262.51±4.90
LDH 3	-97.99±2.70	-172.64±5.03	-46.25±2.70	251.38±5.03	24.48	275.86±5.03
LDH 4	-69.49±3.63	-146.84±3.87	-25.72±3.63	192.85±3.86	40.46	233.31±3.86
LDH 5	-111.39±3.71	-157.61±3.68	-64.40±3.71	183.57±3.69	37.22	220.74±3.67

This is the peer-reviewed, final accepted version for American Mineralogist, published by the Mineralogical Society of America.
The published version is subject to change. Cite as Authors (Year) Title. American Mineralogist, in press.
DOI: https://doi.org/10.2138/am-2021-7935. http://www.minsocam.org/

516 Figure 1

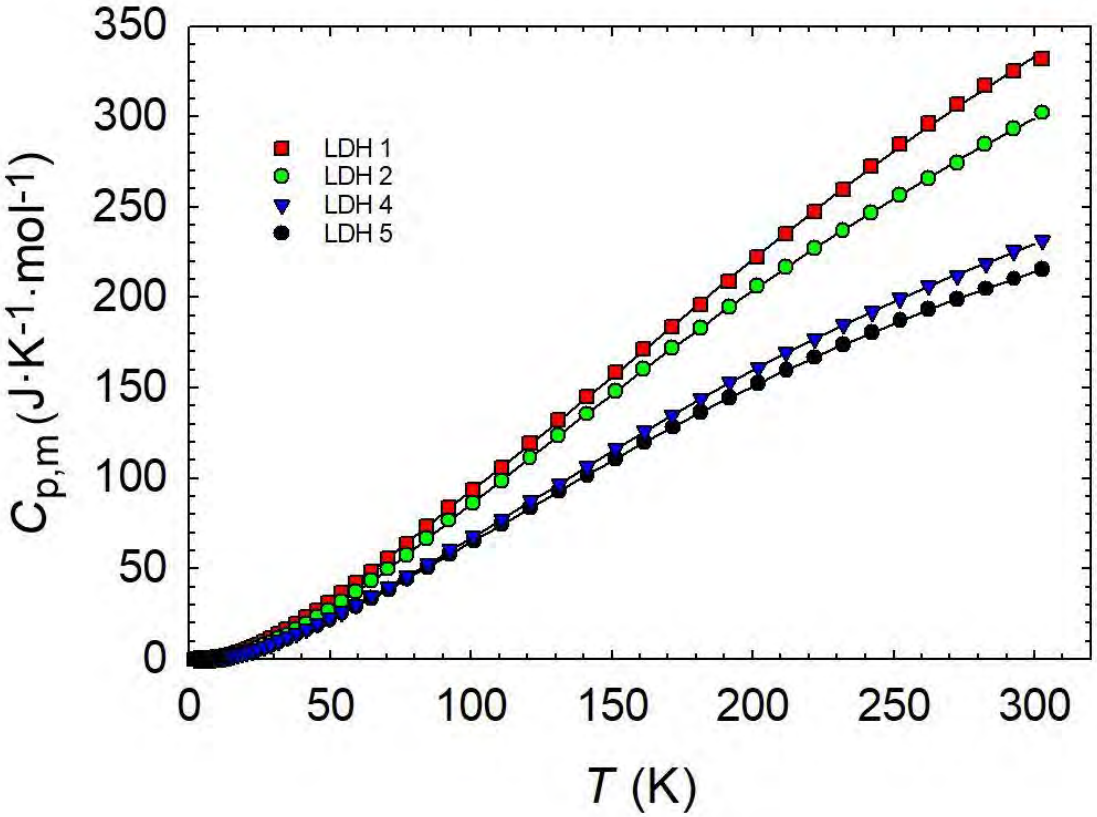

517
518

This is the peer-reviewed, final accepted version for American Mineralogist, published by the Mineralogical Society of America.
The published version is subject to change. Cite as Authors (Year) Title. American Mineralogist, in press.
DOI: https://doi.org/10.2138/am-2021-7935. http://www.minsocam.org/

519 Figure 2

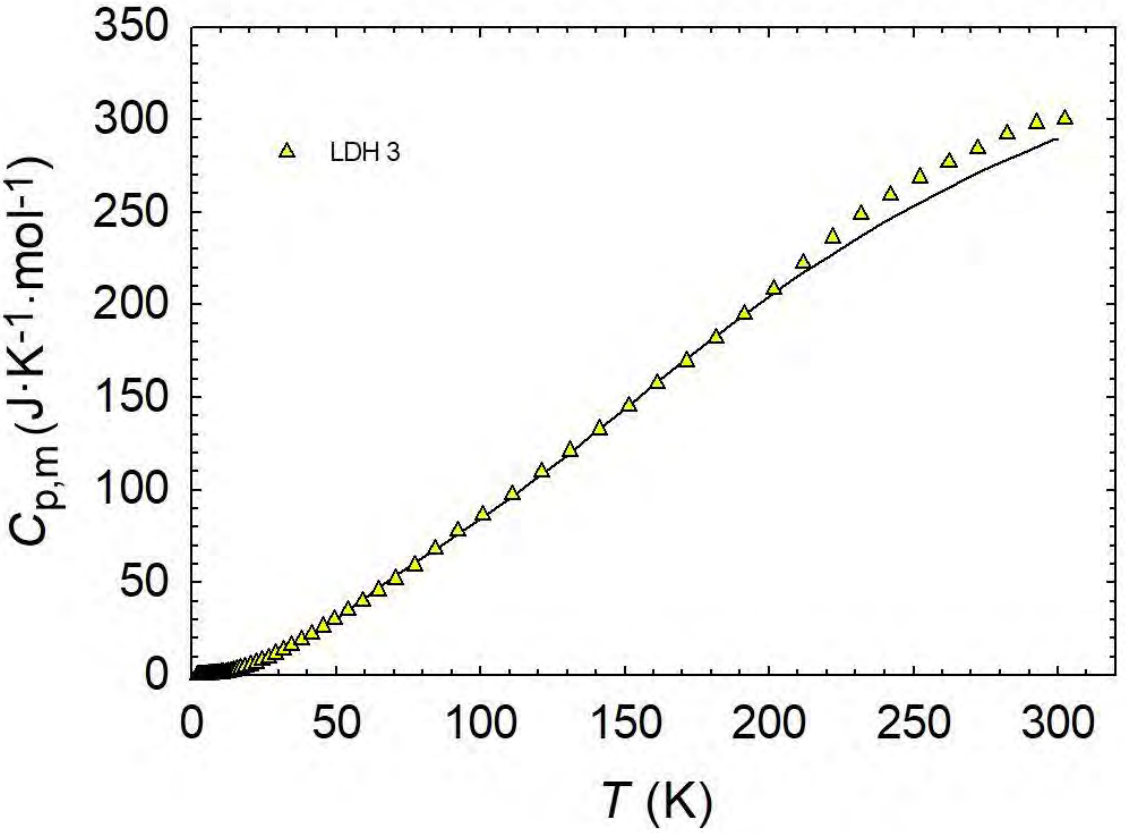

520
521
522
523

This is the peer-reviewed, final accepted version for American Mineralogist, published by the Mineralogical Society of America.
The published version is subject to change. Cite as Authors (Year) Title. American Mineralogist, in press.
DOI: https://doi.org/10.2138/am-2021-7935. http://www.minsocam.org/

524 Figure 3

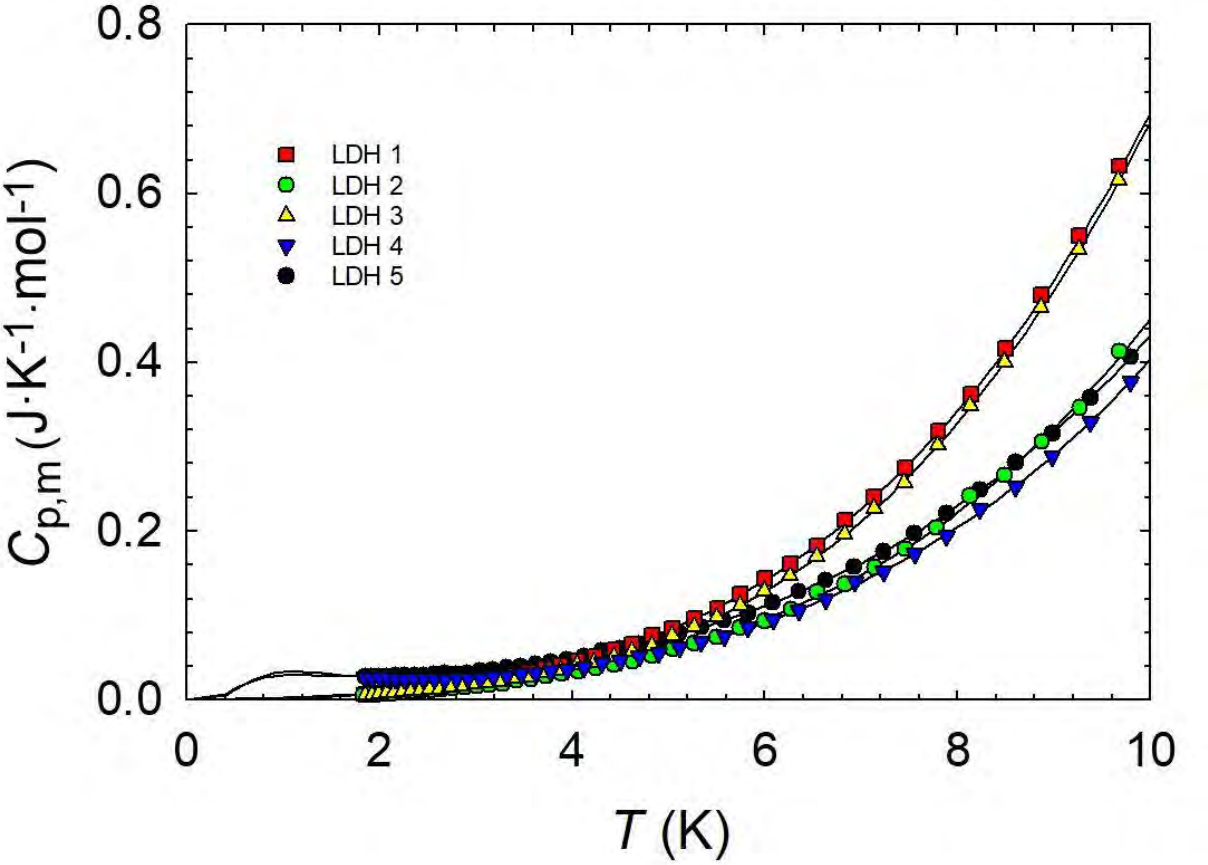

525
526

527 Figure 4

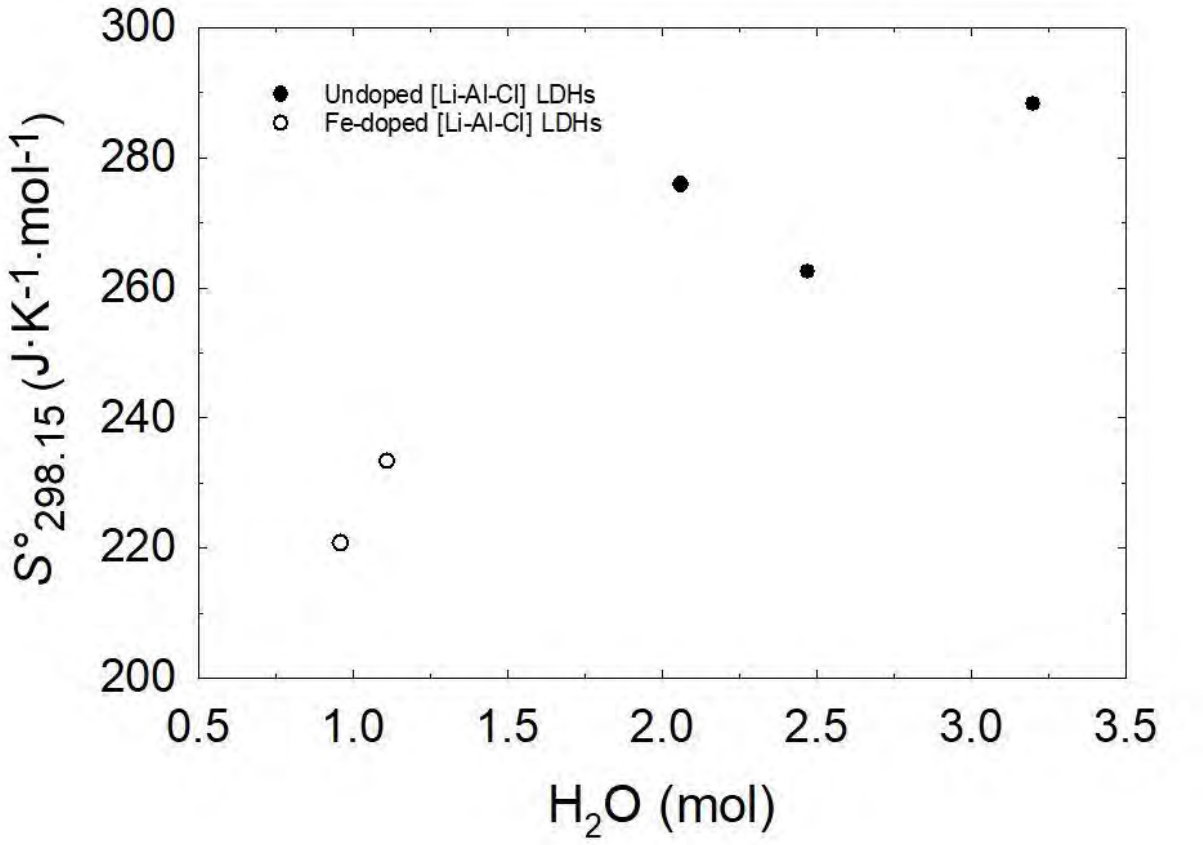

528
529